Automotive Science and Engineering, Vol. 12, No. 2, (2022), 3860-3872

Iran University of Science and Technology

Automotive Science and Engineering

Journal Homepage: ase.iust.ac.ir

ISSN: 2008-9899

Investigating the construction of three-way connection tubes for hydraulic systems in vehicles by dynamic-impact loading in hydroforming

Arman Mohseni [1], Javad Rezapour [1,*], Sina Gohari Rad[2], Reza Rajabiehfard[2]

[1] Department of Mechanical Engineering, Lahijan Branch, Islamic Azad University, Lahijan, Iran.

[2] Department of Mechanical Engineering, Rasht Branch, Islamic Azad University, Rasht, Iran.

ARTICLE INFO

Article history

Received: 20 May 2022

Accepted: 19 Jun 2022

Published: 19 Jun 2022

Keywords:

Hydroforming

Internal pressure

Axial feeding

SPH Simulation model

Dynamic loading path

A B S T R A C T

Background: Hydroforming is employed in the manufacture of hollow monolithic products to reduce the number of joints. This method can reduce the weight and enhance the quality of fluid transfer parts in a vehicle's hydraulic system. Hydroforming is a process in which parts are formed into the shape of a mold using fluid pressure. An important issue in this process is adopting an optimal loading path. **Methods:** In the present research, a drop hammer was used to implement the dynamic loading path in the tests. This hammer lowers the number of systems to use and reduces the testing time. Accordingly, a single energy source was used simultaneously to provide axial feeding and internal pressure. To this end, designing a mold suitable for the dynamic loading path was necessary. **Results:** This numerical study investigates tubes' deformation based on the applied impact and the amount of fluid in the mold. Moreover, axial feeding was provided with the help of different punches on the sides of the tube. Hence, the kinetic energy, amount of fluid, sealing, lubrication, and the material and thickness of the tube must be proportional for the correct forming of the tube. The hydrodynamic loading path can be studied using simulation. Thus, ABAQUS software was employed to observe the changes resulting from the process. From the smoothed-particle hydrodynamics perspective, it is a meshless method based on interpolation that uses a particle system to examine the system state and predict fields such as displacement, stress, and pressure. Moreover, several simulation results were examined for results accuracy to ensure convergence of the solution. **Conclusions:** One of the main observations of this research is that selecting side punches with a smaller central hole radius is proportional to the kinetic energy and the amount of fluid. Moreover, it can be effective in achieving the optimal loading path.

*Corresponding Author
Email Address: javad.rs82@gmail.com
https://doi.org/10.22068/ase.2022.612

1. Introduction

Hydroforming has various industrial applications in manufacturing strong lightweight parts. It is applied to form hollow metal parts into straight or bent, simple or complex shapes via an internal hydraulic pressure and an axial force. The concept of hydroforming was developed from the need to manufacture a product with different geometries from parts with shape and dimensional limitations for part of the production process in a project. Since more material flexibility is available in hydroforming, using strong and thin materials effectively reduces the weight of the manufactured part. Hydroforming is a significant solution for minimizing the number of connections and maximizing integrity. It has remarkable advantages, such as higher smoothness, fewer secondary operations, less discard, higher dimensional accuracy, lower tool erosion, lack of need for several molds, shorter production time, and a smaller production cost over other methods.

An important factor in quality improvement in hydroforming is the loading path. This path is determined by specifying the references for applying force and pressure during the process. In hydroforming, adjusting the important parameters to obtain the desired parts and correctly implementing the loading path plays a key role in enhancing the product quality. These parameters are the internal pressure, displacement of the axial punches for axial feeding, and counter punch effect. The industrial manufacturing applications of this method can be found in aircraft manufacturing, healthcare, and automotive industries. The hydroforming process is carried out through internal pressure by an incompressible fluid and axial feeding to prevent strong thinning. Extensive research has been conducted on hydroforming techniques, some of which are presented in the following.

Ahmad Gunaidin et al. [1] experimentally studied the use of reinforcement in hydroforming. They concluded that useful extra pressure is not applied with an excessive increase in the piston motion. Hence, more fluid must be pumped to improve the loading path, requiring a larger mold and higher cost. These authors also considered the thickness distribution and completion of the forming process according to the mold design via calibration pressure. The process is also employed in the mass production of plate heat exchangers, white goods, and automobiles because of its low cost, among other advantages.

Ashrafi et al. [2] employed the concept of an internal mechanical constraint to contain the wrinkle defect in hydroforming to conduct empirical and numerical analyses and obtained test results for identical conditions with a stable internal pressure. Moreover, they considered the wrinkle length as a criterion for confirming the effect of the constraint. The achieved results were a slight increase in the bulge height, wrinkle removal, and better thickness distribution.

Chan et al. [3] adopted a hydroforming method to improve the thickness of variable-diameter tube-shaped parts. In this method, optimizing the loading path was translated to finding the appropriate relationship between the internal pressure and the axial feeding. To this end, the behavior of the part's surface during the process was studied to obtain the optimal thickness displacement in the manufactured part by removing the wrinkles in the deformed tube. This process was conducted to determine the difference between the maximum and minimum thickness of the hydroformed tube.

Christina et al. [4] observed the influence of elastic parameters of the tested material and investigated the factors improving the deformations. The final product's geometry and mechanical properties were important factors in determining the loading path that resulted in the optimal formation of the part according to the mold shape.

Feng et al. [5] considered the maximum internal pressure and axial feeding using the trial and error technique in manufacturing a T-shaped tube. Their selection was based on the deterministic relationships introduced in other studies and the common friction coefficient between the tube and mold surfaces. Accordingly, the numerical and empirical results were compared to determine the optimal loading path. The results indicated a decrease in

thickness with an increase in internal pressure. However, this report may be unique to the tube tested under the specified conditions. As lightweight technology becomes more common in the automotive industry, tube hydroforming gains popularity in producing complex tubular structural components. It takes tubes as objects to form geometry parts in one procedure and produces high-quality seamless tube joints. These tubes can be used in the air intake system, train power system, sea pipeline system, etc.

Gaushen et al. [6] investigated the effect of pressure in the hot hydroforming of an aluminum plate. They stated that a low-rate pressure increases the forming region. In addition, they reported that a temperature rise positively affects this property. In other words, it enhanced the forming process in hydroforming.

Dardayi et al. [7] investigated the geometric parameters affecting tube hydroforming while seeking to maximize the bulge height. They discussed the optimal friction coefficient and a lower internal pressure versus a higher axial feeding. Moreover, they stated that the application of axial feeding application must be near the center of the start of the bulge. However, it also depends on the part's final geometry and initial length.

Guo et al. [8] conducted numerical and experimental studies on hydroforming coated double layer T-shaped tubes. They aimed at determining the optimal loading path based on the ideal internal pressure according to axial feeding. For this purpose, they followed the trial and error method with a friction coefficient of 0.1. The numerical analyses were performed based on finite element method (FEM) modeling. Furthermore, they presented the absence of cracks and wrinkles as an indicator of optimal deformation. These authors expressed the optimal axial feeding as a force along the axial direction of the tube to compensate for the thinning due to internal pressure even if the optimal bulge height is smaller than the maximum one.

Inspired by the idea of a device for high-speed hydroforming, Hermes et al. [9] installed a high-voltage hydraulic power supply on the forming tool and utilized an intermediary for driving the axial punches for axial feeding. They validated their experimental results using a simulated model considering the strain rate. In addition, they compared their results with those of a quasi-static hydroforming process. Research has shown that the deformation rate of the tube and the increase in its diameter depend on the fluid pressure rate. The authors highlighted the significance of a pressure rate control factor for improving the forming. Hydroforming has long been a significant production technology. This technology allows manufacturers to produce complex thin-walled and lightweight automotive components in a single step on special production machines.

Jianping et al. [10] studied the effect of friction on hydroforming under different loading paths. Eventually, they obtained a relationship between the friction coefficient and the effective fluid pressure rate. They also introduced a relationship between the ratio of the fluid speed and the axial feeding speed based on their observations under various conditions.

A challenge in understanding and introducing a suitable criterion for forming is expressing the desired deformation parameter, according to which the appropriate loading path is determined. Therefore, a condition must be specified to detect the optimal loading path and implement it accurately. For instance, Reddy et al. [11] presented the smallest reduction in the thickness distribution at the bulge location as a criterion for suitable forming. Although some researchers have considered the variations in thickness as an indicator of the suitability of the forming process, the basis for recognizing an appropriate thickness distribution and representing the acceptable deformation remains to be determined. Moreover, this criterion can be selected based on the type of loading path. As mentioned previously, a uniform reduction in thickness in every region of the part after deformation can be considered a thickness distribution criterion. The optimal reduction has been stated to be about 40% in some studies [12]. Furthermore, some works have introduced the minimization of thickness variations as an indicator for the optimal loading path among all solutions for the final part [13].

Hence, the following can be named as criteria for acceptable deformation:

1- Maximum deformation corresponding to the internal mold shape [14]

2- Suitable thickness distribution [11-13]

3- Absence of wrinkles, thinning, and fracture [14]

4- Bulge quality based on thickness distribution [11]

The present paper numerically investigates the manufacture of a T-shaped aluminum tube using ABAQUS software. The loading path specified for this research is in the dynamic approach and is applied in the form of a low-rate impact. A drop hammer was used for experimental purposes by designing the mold in such a way that an impact can establish a sudden internal pressure and axial feeding. Thus, similar conditions were considered in the simulated model for implementing the dynamic loading path. The numerical results were compared with the experimental results in the previous research by the authors of the present paper [15]. Important factors considered in this study are the thickness distribution and the change in length of the tube. They will be compared to a simulation different from [15] to validate the experimental method by numerically examining it. Finally, the effects of tube geometry and axial feeding on the dynamic loading path will be investigated by adopting a different initial tube thickness and changing the hole diameter of the axial punch. it is worth noting that Surface quality consists of two main aspects which are surface integrity and surface topography [16].

2. Experimental setup

This paper simulates tubes deformed at a low rate by a drop hammer. A schematic of the setup is displayed in Fig. 1. Also, a schematic of the test preparation for tube forming using the incompressible fluid inside the mold is presented in Fig. 2. The experimental procedure is described in detail in [15].

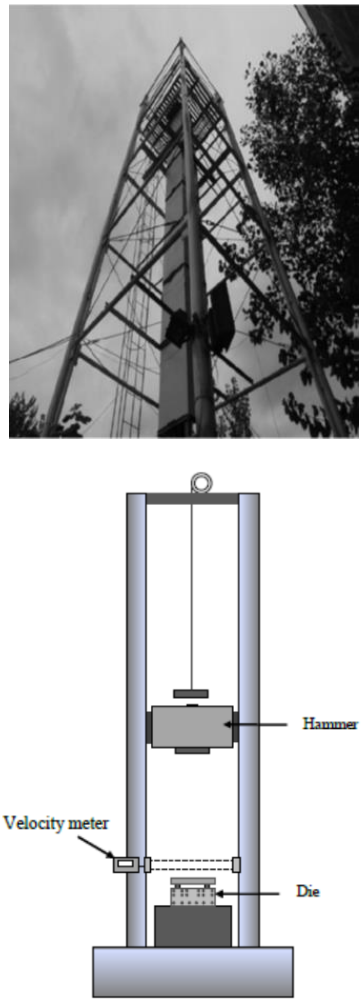

Figure 1: Schematic image of a drop hammer with a device located in Ahrar university

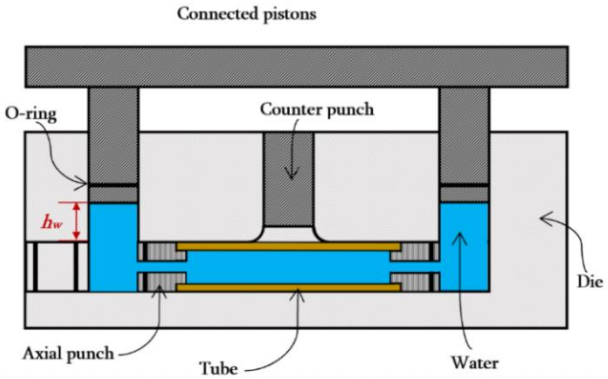

Figure 2: Schematic of the preparation of the tube inside the mold containing the fluid for the deformation process

The kinetic energy resulting from the collision between the drop hammer and the connected

pistons creates a hydrodynamic pressure inside the mold, resulting in the deformation. Besides, the axial feeding can be provided through the axial punches on the sides of the tube. The dynamic pressure wave of the fluid penetrates through the central hole in the punch. This pressure wave can be defined as the cause of the increase in the bulge regarding its effect on the internal tube surface. Moreover, a counter punch was employed to complete the calibration pressure. Fig. 3 depicts a view of the axial punches with a central hole diameter of 2.5 mm used in the tests. The mold shown in Fig. 4 was selected for appropriate use with the dynamic loading for tube hydroforming.

The initial conditions of the tested tubes are presented in Table 1 and Fig. 5, which display the geometric and mechanical properties of the aluminum tube.

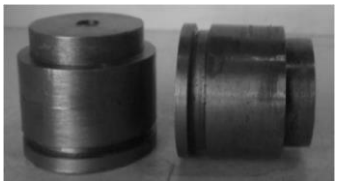

Figure 3: Axial punches

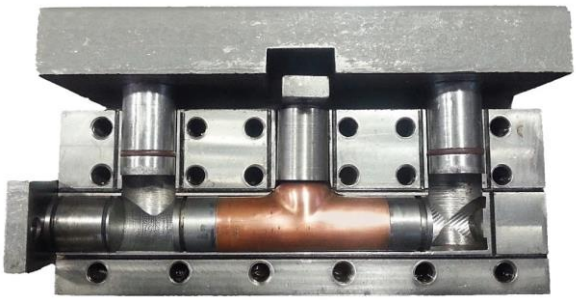

Figure 4: Image of the mold used in the experiments

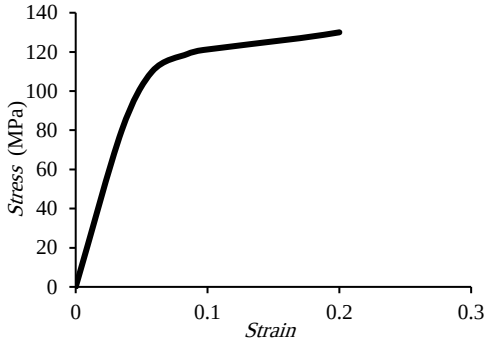

Figure 5: Stress-strain diagram expressing the mechanical properties of aluminum tube

Table 1: Geometric specifications of aluminum tubes

Quantity	parameters
25	Diameter
2.8 , 2.1	Thickness
80	First length
700	Young modulus
2700	Density

As explained before, dynamic hydroforming is used for the experimental study of the manufacture of T-shaped aluminum tubes. The post-forming changes for this loading path are reported in Table 2.

This paper presents a simulation model and validates it based on the experimental observation in [15]. Second, a different numerical analysis is introduced to make a more accurate comparison between the simulation results in [15] and the test results. Third, we compare new points for changes due to forming in this research, including a tube with a different initial thickness and a punch with a different center hole diameter, leading to changes in the loading. Finally, its effects on the loading path will be investigated.

The following examines the simulation according to the tests.

3. Modeling and numerical results

In real engineering practice, there exist varieties of typical sources of uncertainty that have to be compensated through a simulation approach. The structured uncertainty concerns about the model uncertainty due to unknown values of parameters in a known structure [17 and 18]. The method used for this purpose, called smoothed-particle hydrodynamics (SPH), is meshless and based on interpolation.

Table 2: Result of aluminum tube experiments [15]

Test	h_w	Kinetic energy	Length decrease	Bulge
T.1	12	210	1.4	2.2
T.2	18	285	2	5.6
T.3	13	190	1.3	4.6
T.4	13	285	1.6	5.3
T.5	13	327	1.8	5.4
T.6	14	327	2	5.8
T.7	20	306	2.2	6.4

It uses particle systems to investigate the system state and predict fields such as displacement, velocity, stress, density, and pressure. This method integrates each field Q_m for each particle (m^{th} particle) up to adjacent particles, as shown in Eq. (1):

$$Q_m = \int Q_n W\left(r_{mn}, h\right) dV \tag{1}$$

where W is the smooth or kernel function, h represents the smooth distance identifying the range of influence of the particle, r_{mn} expresses the distance between each particle and adjacent particles, and V denotes volume. The kernel function contains several conditions, including the normality, Dirac delta condition, and compactness. The following equations represent these conditions in the order of their appearance:

$$\int W\left(r_{mn}, h\right) dV = 1 \tag{2}$$

$$\lim_{h\to 0} W\left(r_{mn}, h\right) = \delta_{mn} = \begin{cases} 1, & m = n \\ 0, & m \neq n \end{cases} \tag{3}$$

$$W\left(r_{mn}, h\right) = 0 \quad ; \left|r_{mn}\right| \geq \alpha h \tag{4}$$

where α represents a constant taken according to the kernel function and determines the range of influence of this function. There are a large number of smooth functions, including the bell curve, Gaussian function, edge cube, and other higher-order functions. For instance, the value of α for the cube function is considered to be 2. Fig. 6 depicts a schematic of this function, while Eq. (5) expresses this function mathematically.

$$W\left(r_{mn}, h\right) = \frac{N(i)}{h^i} \begin{cases} 1 - \frac{3}{2}\alpha^2 + \frac{3}{4}\alpha^3 & \left|\alpha\right| \leq 1 \\ \frac{3}{2}(2-\alpha)^2 & 1 < \left|\alpha\right| \leq 2 \\ 0 & 2 < \left|\alpha\right| \end{cases} \tag{5}$$

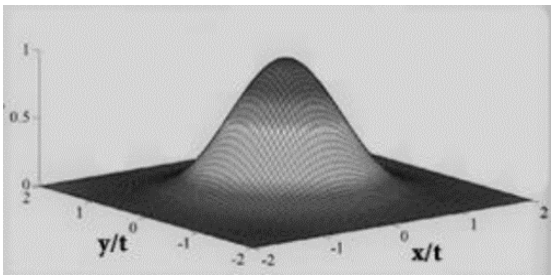

Figure 6: Kernel function diagram

where r_{mn}/h shows the normalization factor of the kernel function. In addition, N(i) is expressed by Eq. (6).

$$N(i) = \left\{ \frac{2}{3}, \frac{10\Pi}{7}, \frac{1}{\Pi}, \frac{70\Pi^2}{31}, \frac{5\Pi^2}{31} \right\} \quad ; \quad i = 1, \ldots, 5 \tag{6}$$

Fig. 7 shows a schematic of the particles and the range of influence of the field specified in this method.

Subsequently, Eq. (1) can be rewritten in the following discrete form (Eq. 7):

$$Q_m = \sum_{n=1}^{N_n} Q_n W\left(r_{mn}, h\right) V_n \tag{7}$$

Here, N_n denotes the number of particles adjacent to the n^{th} particle, and V represents the volume. Substituting the density relationship into Eq. (8) results in Eq. (9).

$$\rho_n = \frac{M_n}{V_n} \tag{8}$$

$$Q_m = \sum_{n=1}^{N_n} Q_n W\left(r_{mn}, h\right) \frac{M_n}{\rho_n} \tag{9}$$

where M_n and ρ_n are the weight and density of the n^{th} particle, respectively.

Moreover, the existence of a particle dynamics computational algorithm in the explicit approach in ABAQUS has enabled modeling the intermediate fluid using the smoothed particle hydrodynamics method.

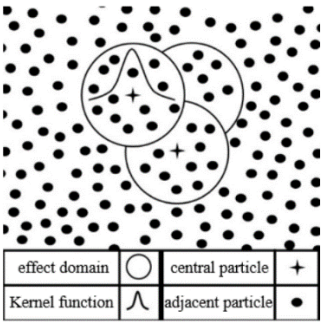

Figure 7: Schematic of particle system and effect domain

3.1. Geometry and meshing of the coupled model

In this method, the fluid particles and the tube elements under loading are coupled by modeling the test in ABAQUS 6.14.

The process is simulated using the elements found in the ABAQUS library for different geometric models. In this model, C3D8R elements, which represent elements with a reduced formulation and can control the hourglass phenomenon, are used to model the loaded tube. Each set of elements in ABAQUS possesses a specific formulation based on which the FEM modeling is carried out. The order of the element and the manner of numerical integration directly affect the solution accuracy of an analysis. Fully integrated elements refer to the number of Gauss points required for integrating the polynomials in the stiffness matrix related to an element with a right corner. The right corners refer to the smoothness of the edges and the perpendicularity of the angles in the element. Due to shear locking, these elements must be used in loadings with minimum bending. Hence, introducing an alternative solution aimed at analyzing bending problems seems necessary. One particular design consists of elements with reduced integration points, known as reduced-integration elements [19]. Fig. 8 displays these two elements. Several simulation solutions were examined in this study to determine the element size that results in convergence and best accuracy. Accordingly, the number of elements for the simulation was considered 501,760. The ABAQUS software applies particle elements for modeling fluids using the smoothed-particle hydrodynamics technique. A general view of the particles modeled in this way is shown in Fig. 9.

Some elements (e.g., contact elements, distributed couple, and particle elements) are not supported by the software and must be created outside the mesh module. The 'inp' file generated in the 'Job module' must be used for including these elements in the solution process. Moreover, the other components (e.g., the water container, piston, and mold) must be modeled as rigid and meshed using an appropriate number of elements. The rigid components were modeled in discrete form since rigid elements must be meshed in metal forming problems due to the contact conditions between the members [19]. The tube was modeled as a deformable solid in the geometry section of the software. Fig. 10 shows the corresponding mesh. Given the type of test carried out (release of a hammer weight from a specified height for tube forming), the available parameters are the drop hammer's energy, mass, and speed upon collision. Since the strain rate is a significant parameter in metal forming problems, the speed parameter is suitable input for the solution.

Considering all the measurable parameters in the test, the kinetic energy and the amount of fluid are of great significance to the model. The test was accurately modeled by assigning the hammer mass and collision speed obtained from a laser tachometer.

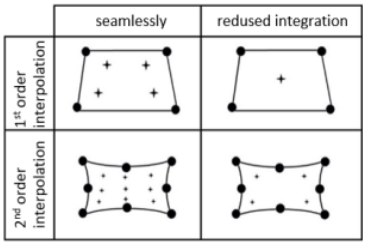

Figure 8: integrated and reducing elements

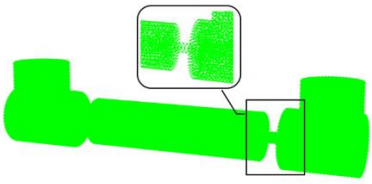

Figure 9: Particles modeled by smooth particle hydrodynamics

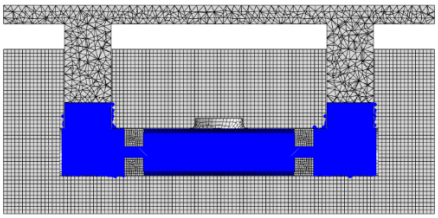

Figure 10: finite element view of mold

The 'Interaction' module can determine the mentioned parameters if the problem includes part contact, component interaction, DOF constraints, and relationship and constraint definition. ABAQUS can detect contact between two or more members if only the user has already defined the mechanical properties of the contact, involved parts, and other specifications in the 'Interaction' module. The interaction between various parts of the system and the part surfaces was defined with a friction coefficient of 0.1.

3.2. Simulation results

In this section, the simulation results are numerically studied according to the descriptions presented for the testing and corresponding modeling procedure. To this end, first, the experimental results will be compared with the numerical outcome. Then, the method proposed in this research is validated using the modeling results from [15]. Afterward, new studies on the effect of changes in the axial punches and the tube thickness are presented. The significance of these studies lies in their ability to predict the test results. The presented points are examined from several aspects.

Fig. 11 represents the simulated and experimental models of the deformed aluminum tube from Test T4. A good agreement between the results is observed in this figure.

As shown in Fig. 12, some points were selected to verify the model in the previous research and examine the validity of the numerical results using the mentioned test. Also, using these points allowed comparing the accuracy of the new simulation with that of the past one. After the verification, the thickness effect can be observed for the 2.8-mm thick tubes. These points are provided in Table 3. As shown in this table, a good agreement exists between the test and the old and new models. This consistency indicates the higher accuracy obtained using the new model than the previous FEM. Based on this research, a thickness reduction smaller than 35% was reported at Point D for the 2.1-mm tube. However, this decrease is about 55% for the 2.8-mm tube under identical conditions. Hence, the tube with the smaller initial thickness produced better results.

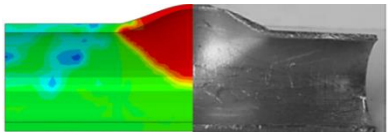

Figure 11: View of the simulated and experimental model of the deformed aluminum tube in Experiment T.4

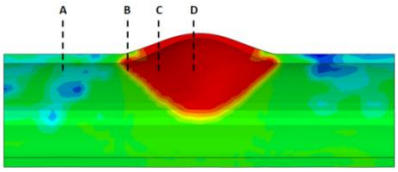

Figure 12: Different points to determine the thickness of the deformed aluminum tube in Experiment T.4 (SPH)

Table 3: Investigation of thickness changes at any point for two pipes according to experiments and validation of simulations (same conditions T.4) [15]

Spot	Experimental (mm)	FEM th 2.1 (mm)	SPH th 2.1 (mm)	SPH th 2.8 (mm)
A	2	2	2	2.72
B	1.78	1.86	1.74	2.54
C	1.56	1.35	1.48	2.16
D	0.8	1	0.73	1.55

Fig. 13 shows the deformed tube sample T5 [15] (based on Table 2). Also, Fig. 14 illustrates that the changes in force versus time obtained from the two models for the 2.1 mm thickness are in good agreement. Moreover, a larger force is required for axial feeding for the 2.8 mm thickness. This result shows that a larger initial thickness leads to a larger force received for axial feeding.

Fig. 15 displays the changes in pressure versus time. According to this figure, back pressure occurred for the 2.8 mm thickness. This pressure can be due to the repulsion of the axial punches in a fraction of a second and the continuation of the formation at a higher pressure. This result already seems obvious given the larger thickness of the original tube. According to Table 4, the new model is validated compared to the simulation of the previous research. Also, the higher accuracy of the present model (smoothed-particle hydrodynamics) compared to [15] is demonstrated based on measurements of the test samples. In addition, the impact of a larger initial thickness and a change in the diameter of the center hole of the axial punch is clearly specified. An increase in the tube thickness increases resistance to longitudinal changes. On the other hand, reducing the cross-sectional area of the axial punch (i.e., change in the diameter of the center hole from 2.5 mm to 3.4 mm) results in smaller axial feeding. In other words, a smaller axial punch hole can lead to a better thickness distribution in this sample.

Figure 13: deformed tube (sample T.5, thickness of 2.1 mm) [15]

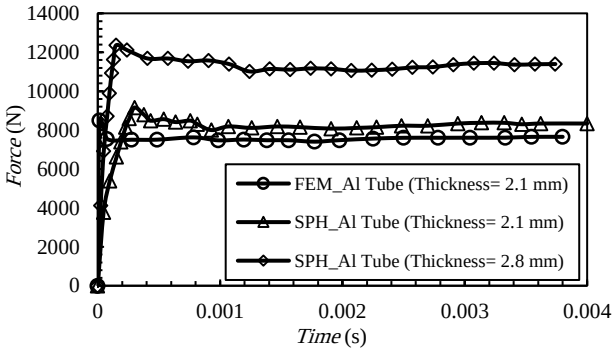

Figure 14: Force – Time diagram (condition T.5, axial punch 2.5 mm)

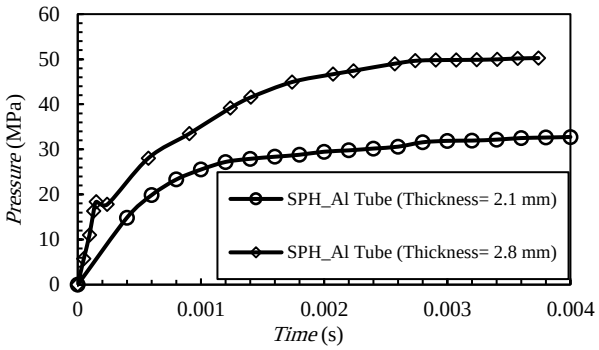

Figure 15: pressure – time diagram for aluminum tube in two different thicknesses for same condition of T.5 and axial punch 2.5mm

Table 4: Effect of axial punch for different initial thickness on axial changes (same conditions T.5)

Axial punch radius (mm)	experimental (mm)	FEM th 2.1 (mm)	SPH th 2.1 (mm)	SPH th 2.8 (mm)
2.5	0.9	1.4	0.82	0.71
3.4	-	-	0.61	0.43

Fig. 16 confirms the last table's results by showing the bulge height versus the axial feeding. According to this figure, selecting an axial punch with a smaller radius results in better axial feeding and bulge height. Moreover, the effect of the axial punch on the thickness distribution can be observed in Fig. 17. This figure also shows that using a smaller axial punch diameter can lead to a better thickness distribution in the forming process. Furthermore, this point is demonstrated in two different paths, which present more bulge height.

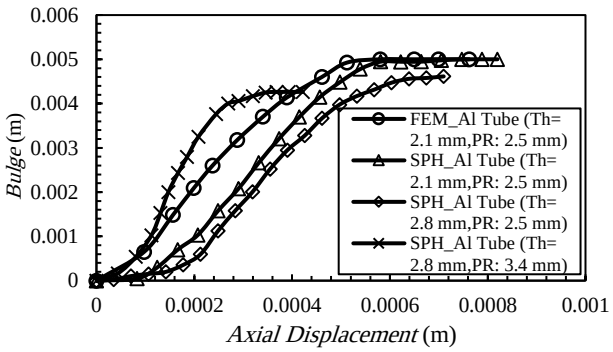

Figure 16: Bulge – axial displacement diagram for T.5 condition

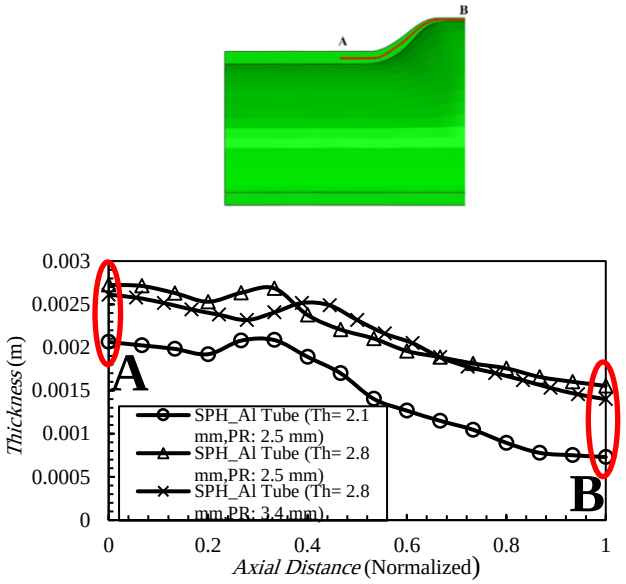

Figure 17: thickness distribution in axial distance for T.5 condition

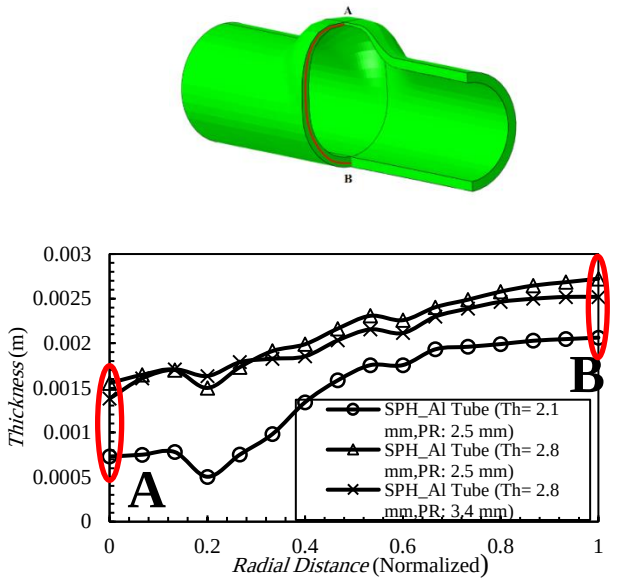

Figure 18: thickness distribution in radial distance for T.5 condition

Fig. 18 demonstrates the discussed points in the radial direction by showing their similar behaviors in the graph. Moreover, it proves these points by the positive effect of the axial feeding on the thickness distribution and a larger bulge height for the punch with a smaller radius.

Given that various aspects of changes and the effects of different factors on the forming process were studied, the prediction feasibility of this simulation model is addressed. Fig. 19 displays the deformation process. Also, Table 5 shows the relationship between the kinetic energy values and the internal pressure and axial force for the bulge height of 5 mm and a fluid column of 15 mm.

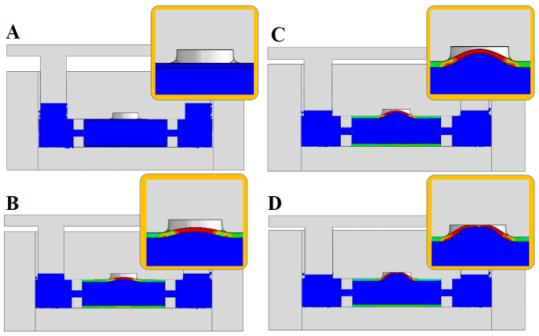

Figure 19: The process of deformation of tube with thickness of 2.8mm

Table 5: Values of different parameters obtained from simulation predictions for tube with thickness 2.8 mm

Axial punch radius (mm)	(mm)bulge	h_w (mm)	Kinetic (J) energy	Max internal pressure (Pa)	Max axial (kN) force	Max th reduction (%)
2.5	5	15	539.55	56.35	15.28	35.43
3.4	5	15	458.62	61.38	14.53	38.56

The table 5 shows the loading path that provides the best thickness distribution given different axial punches. Furthermore, as demonstrated in previous tests, the axial punch with a smaller center hole results in better deformation also for this sample (which is a prediction of SPH T.P). Therefore, a good agreement is observed between the axial punch outcomes under different conditions.

4. Discussion

The main points extracted regarding the test results and the corresponding numerical validation are as follows:

1- In the dynamic hydroforming approach, wrinkles in the form of slight increases in

thickness were observed at the vertices (Fig. 17).

2- Any small change in the inputs (e.g., kinetic energy, axial punch conditions, and fluid column height) leads to significant changes in the process results.

3- The initial tube thickness is an important parameter that considerably affects this process.

4- Low-velocity impact hydroforming was performed by applying kinetic energy using a drop hammer, i.e., low-rate forming. This process can also be carried out rapidly with high power.

5- Selecting a suitable amount of fluid in terms of the input kinetic energy produces an optimized deformed tube.

6- The method used to simulate the fluid flow correctly revealed details in the numerical study and presented test prediction feasibility.

7- In this method, deformation, thickness distribution, and the start and completion of deformation can be observed with acceptable accuracy.

8- The internal pressure and axial feeding values must be considered the inputs of older simulation approaches. However, in the present simulation, the internal pressure and axial force (affected by the axial punch) can be predicted in every loading according to the significance of the amount of fluid and kinetic energy based on the verifications.

9- In case the diameter of the center hole of the axial punch changes and the bulge height and fluid column height are kept constant, different kinetic energy is required to achieve common results. Also, a larger internal pressure was reported in the numerical study with a larger axial punch even if smaller kinetic energy was received. This result can be interpreted as a weaker thickness distribution (Table 5).

10- A suitable proportion between the fluid amount and kinetic energy makes it possible to obtain an appropriate axial feeding and leads to an optimal loading path.

11- The tube with the smaller initial thickness under T4 conditions [15] was observed to undergo better forming.

12- Employing an axial punch with a smaller center hole resulted in better axial feeding in the numerical study of the T5 sample.

13- Comparing the T.4 and T.5 samples shows that higher kinetic energy with an identical fluid column height in the aluminum tube caused a larger deformation (with an identical axial punch).

14- The SPH T.P sample (which represents the model that predicts the internal pressure, axial force, and thickness reduction values) agrees well with these discussions.

15- By choosing the loading path leading to a 35% reduction in thickness (Table 5), one can use T-shaped fittings to branch and redirect the fluid in a vehicle's hydraulic system. The present research discusses how to approach suitable internal pressure and axial feeding values and expresses it using parameters such as initial tube thickness, axial punch geometry, kinetic energy, and fluid column.

16- Given the high speed of the process, it is possible to improve the quantitative and qualitative efficiency of manufacturing hydraulic fitting components.

5. Conclusion

This numerical study investigates tubes' deformation based on the applied impact and the amount of fluid in the mold. Also, it provides axial feeding using different punches on the sides of the tube. According to the obtained results, a smaller axial punch center hole diameter with a larger fluid column height produces better results. In addition, it is important to select a tube with a smaller initial thickness. Meanwhile, all the factors must be proportional to each other. Comparing these points demonstrates the validity of the results.

Another important point observed in the SPH T.P samples is that the internal pressure does not depend merely on the fluid column height and the kinetic energy but also on the radius of the center hole of the axial punch. Although the fluid column is the same as the one shown in Table 5, a smaller internal pressure was reported for a smaller center hole diameter, despite larger kinetic energy being applied. This result can be attributed to the flow of extra fluid in a shorter time in the case of the punch with a larger center hole. Furthermore, using the punch with a larger center hole declines the risk of wrinkling during the deformation, although it does not optimize the overall process.

Moreover, the largest thickness reduction in this sample is smaller than 40%, which indicates good deformation.

Another parameter that leads to an optimal manufactured part is selecting more ductile tubes, thereby facilitating the examinations for determining the loading path.

Declaration of Conflicting Interests

The author(s) declared no potential conflicts of interest with respect to the research, authorship, and/or publication of this article.

References

[1] A. Günaydın, M. Halkacı, F. Ateş, H. Selçuk, Experimental Research of the Usability on Double Acting Intensifiers in Hydroforming, MATEC Web of Conferences, (January 2018).

[2] H. Faraji, Kh. Khalili, A. Ashrafi, The Use of Internal Mechanical Insert to Prevent Wrinkling Defects in T-joint Hydroforming Process, Modares Mechanical Engineering, Vol. 8, No. 19, (2019), pp. 1989-2000. (in Persian)

[3] C. Han, Q. Liu, H. Lu, G. L.Gao, W. C. Xie, S. J. Yuan, Thickness improvement in hydroforming of a variable diameter tubular component by using wrinkles and preforms, The International Journal of Advanced Manufacturing Technology, Vol. 99, No. 9-11, (2018), pp. 2993-3003.

[4] C. Churiaque, J. Amaya, F. Caamano, J. Martinez, J. Botana, Springback Estimation in the Hydroforming Process of UNS A92024 T3 Aluminum Alloy by FEM Simulations, Multidisciplinary Digital Publishing Institute, Vol. 8, No. 6, (2018).

[5] F. Ying, Zh. Ge, L. An, W. Lin, Loading path optimization of T tube in hydroforming process using response surface method, The International Journal of Advanced Manufacturing Technology, Vol. 101, No. 5-8, (201), pp. 1979-1995.

[6] G. Cai, Ch. Wu, Z. Gao, L. Lang, S. Alexandrov, Investigation on the effect of pressure rate on formability of aluminum alloy during warm/hot sheet hydroforming, American Institute of Physics, Vol. 8, No. 9, (2018).

[7] H. Dardaei, A. Tekkaya, F. Legat, A. Henke, Investigation of the effects of process and geometrical parameters on formability in tube hydroforming using a modular hydroforming tool, Proceedings of the 21st International ESAFORM Conference on Material Forming, (2018).

[8] X. Guo, Zh. Liu, H. Wang, J. Tao, Hydroforming simulation and experiment of clad T shapes, International Journal of Advanced Manufacturing Technology, Vol. 83, No. 1-4, (2016), pp. 381-387.

[9] M. Hermes, A. keskin, Ch. Berlinger, New Device and Technology for High Speed Hydroforming, 5th International Conference on New Forming Technology, (2018).

[10] J. Ma, L. Fa, Y. He, Dynamic Frictional Characteristics of TP2 Copper Tubes during Hydroforming under Different Loading and Fluid Velocities, Journal of Materials Engineering and Performance, Vol. 28, (2019), pp. 3661-3672.

[11] P. Reddy, B. Reddy, P. Ramulu, An investigation on tube hydroforming process considering the effect of frictional coefficient and corner radius, Advances in Materials and Processing Technologies, Vol. 6, No. 1, (2020), pp. 84-103.

[12] T. Hama, M. Asakawa, H. Fukiharu, A. Makinuchi, Simulation of Hammering Hydroforming by Static Explicit FEM, Iron and Steel Institute of Japan, Vol. 44, No. 1, (2004), pp. 123-128.

[13] J. Yang, B. Jeon, S. lk oh, Design sensitivity analysis and optimization of the hydrofoming process, Journal of Materials Processing Technology, Vol. 113, No. 1-3, (2001), pp. 666-672.

[14] H. Ahmadi, M. Zohoor, Investigation of the effective parameters in tube hydroforming process by using experimental and finite element methodfor manufacturing of tee joint products, The International Journal of Advanced Manufacturing Technology, Vol. 93, No. 1-4, (2017), pp. 393-495.

[15] M. Alitavoli, H. Babaei, A. Mohseni, R. Rajabiehfard, Experimental and numerical forming of T shaped metallic tubes subjected to hydrodynamic loading, Modares Mechanical Engineering, Vol. 16, No. 9, (2016), pp. 223-232. (in Persian)

[16] M. H. Shojaeefard, A. Khalkhali, Sh. Shahbaz, Analysis and optimization of the surface waviness in the single-point incremental sheet metal forming, Journal of Process Mechanical Engineering, Vol. 223, No. 4, (2019), pp. 1-7.

[17] J. Rezapour, P. Afzali, Rollover avoidance in sport utility vehicles: a multi-criteria viewpoint, International Journal of Automotive Research, Vol. 10, No. 3, (2020), pp. 3357-3368.

[18] J. Rezapour, B. Bahramijoo, A. Jamali, N. Nariman-zadeh, Robust multi-objective controller design for vehicle rollover prevention, International Journal of Automotive Engineering, Vol.4, No.4, (2014), pp. 846-856.

[19] M.B. Liu, G. Liu, Smoothed particle hydrodynamics (SPH): an overview and recent developments. Archives of Computational Methods in Engineering, Vol. 1, No. 19, (2010), pp. 25-76.